Peer-reviewed version available at Catalysts 2020, 10, 375; doi:10.3390/catal10040375

Amino-modified silica as effective support of the palladium catalyst of hydrogenation

Adele R. Latypova[1], Maxim D. Lebedev[1], Evgeniy V. Rumyantsev[1], Dmitry V. Filippov[1], Olga V. Lefedova[1], Alexey V. Bykov[2], Valentin Yu. Doluda[1, 2]

[1]Ivanovo State University of Chemistry and Technology, Sheremetevsky ave.7, Ivanovo, Russian Federation

[2]Tver State Technical University, Nab. A. Nikitina 22, Tver, Russian Federation

Abstract

The article describes synthesis of aminoorgano-functionalized silica as a perspective material for catalysis application. The amino groups have electron donor properties valuable for metal chemical state of palladium. So presence of electron donor groups is important for increasing of catalysts stability. The research is devoted to investigation of silica amino-modified support influence on activity and stability of palladium species in 4-nitroaniline hydrogenation process. A series of catalysts with different supports such as SiO_2, SiO_2-C_3H_6-NH_2 (amino-functionalized silica), γ-Al_2O_3 and activated carbon were studied. The catalytic activity was studied in the hydrogenation of 4-nitroaniline to 1,4-phenylenediamine. The catalysts were characterized by scanning electron microscopy, transmission electron microscopy, x-ray photoelectron spectroscopy, Fourier transform infrared spectroscopy and pulse chemisorption of hydrogen. The 5 wt. % Pd/SiO_2-C_3H_6-NH_2 catalyst exhibited the highest catalytic activity for 4-nitroaniline hydrogenation with 100% conversion and 99% selectivity with respect to 1,4-phenylenediamine.

Keywords: sol-gel, amino-functionalized silica, catalyst, activity, hydrogenation.

1. Introduction

Supported catalysts have wide applications in fine organic synthesis [1-4] and industrial synthetic processes of petrochemicals [5-7] and pharmaceuticals production [8-10]. However, in modern catalysis there is still the problem of increasing the activity and selectivity of catalysts, as well as the search for new catalytically active materials [11-16].

Possible ways to increase catalytic activity and selectivity include development of catalysts synthesis methods, optimization of reaction conditions, catalyst modification by different chemical elements and compounds, application of supports and modification of catalyst surface [4,11-14,16-20]. Modification of catalyst support surface is possible solution to increase catalysts activity and stability. Presence of functional groups on support surface has great influence on electronic state of active metal and metal dispersion [21]. The aminopropyl groups presence a unique possibility for further surface modification. Amino groups modified supports are very useful for further surface nucleophilic substitution and

Preprints (www.preprints.org) | NOT PEER-REVIEWED | Posted: 5 March 2020 doi:10.20944/preprints202003.0089.v1

Peer-reviewed version available at Catalysts 2020, 10, 375; doi:10.3390/catal10040375

obtaining the highest metal dispersion and study of this effect is sufficiently novel trend in catalysis [4,19,20,22-25]. A lot of articles are dedicated to application of amino functionalized mesoporous silica in medicine, pharmaceutics and smart materials, however publications on their influence on active metals catalytic properties are fragmental [26-31]. Present study reports synthesis of aminoorgano-functionalized silica immobilized by palladium nanoparticles using sol-gel method. This way allows to synthesize a various hybrid composition materials by one-pot method. For comparison amorphous silica, activated carbon and gamma-alumina were used as supports for palladium particles.

Catalytic activity of synthesized catalysts was tested in 4-nitroaniline hydrogenation **(Figure 1)**. Liquid phase hydrogenation of substituted nitrobenzenes is essential technology for the production of various aromatic amines – key intermediates for manufacturing agrochemicals, isocyanates, pharmaceuticals and dyes [32-35]. The most commonly used catalysts for different hydrogenation processes contains platinum group metals (palladium, platinum, iridium etc.) attached on different supports [33-38]. Palladium nanoparticles were found to be the most active and have high potential for their catalytic application of essential chemical products [33-35]. However catalysts stability is an open issue for such type of the catalyst, therefore development of active and stable catalysts is in focus of current article.

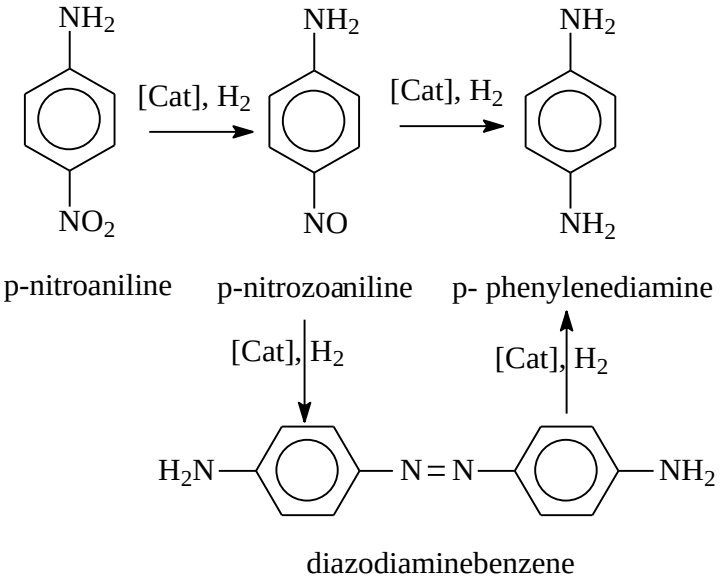

Figure 1. The scheme of 4-nitroaniline hydrogenation to 1,4 phenylenediamine

Preprints (www.preprints.org) | NOT PEER-REVIEWED | Posted: 5 March 2020 doi:10.20944/preprints202003.0089.v1

Peer-reviewed version available at Catalysts 2020, 10, 375; doi:10.3390/catal10040375

Such compounds as 4-nitroaniline are using as industrial raw material to produce of agricultural chemicals, rubber compounding agents, synthetic resin additives, polyamides, pharmaceuticals and dyes. The production of conductive polyamines applicable in electronics [39], also as antioxidants, preservatives [40-42]. The polyamines can find wide application in films materials and membranes due to the biodegradable and electro conductive properties.

2. Results and Discussion

2.1. FTIR spectroscopy of silica supports

The silica modification with aminopropyl groups was studied by Fourier transform infrared spectroscopy **(Figure 2)**. The analysis of FTIR spectra of modified and pure supports revealed the broad bands centered around 3441 cm^{-1} that corresponds to O-H groups vibrations. On the other hand, the spectrum of amino-functionalized silica has peaks at 2940 cm^{-1} and 2886 cm^{-1} assigned to the C-H stretching vibrations of CH- and -CH_2- groups, that can be attributed to the incorporation of the amino group [22,43]. The peak of C–N stretching vibration at 1140 cm^{-1} overlaps with Si-O-Si stretching band in the range 1000–1200 cm^{-1}. The peak of N–H stretching vibration at ~ 3295 cm^{-1} and 3358 cm^{-1} is overlaps with wide peak of stretching vibration at O–H at 3080 cm^{-1} [22,43].

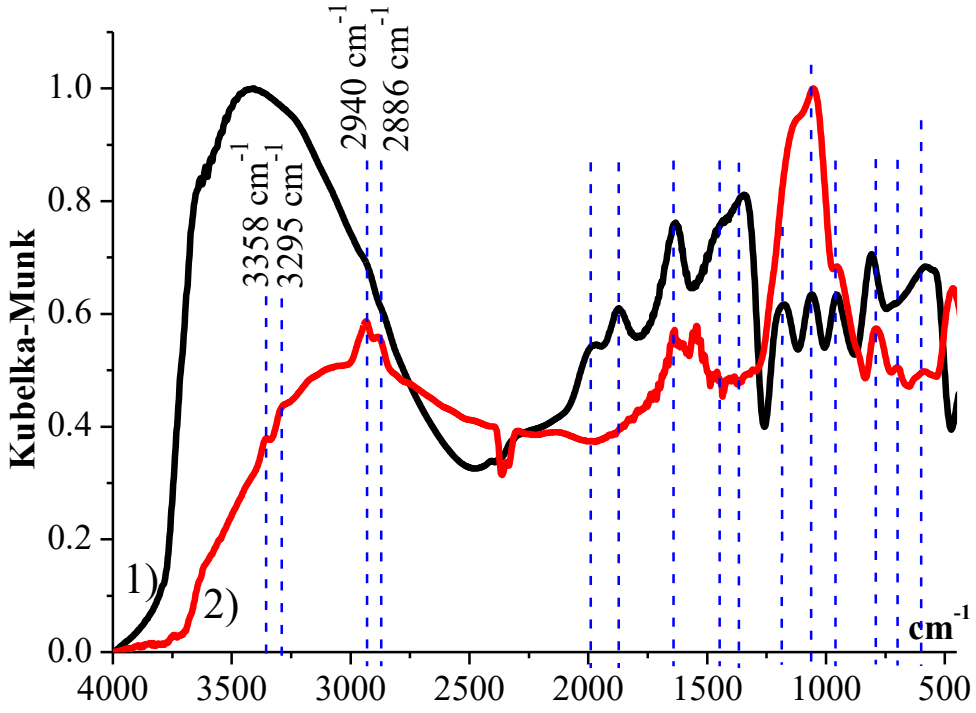

Figure 2. FTIR spectra of supports surface: 1) SiO_2; 2) SiO_2-C_3H_6-NH_2

Peer-reviewed version available at Catalysts 2020, 10, 375; doi:10.3390/catal10040375

The intense bands appearing at 1059, 1176 cm^{-1} were assigned to the asymmetric stretching vibrations Si-O-Si. The symmetric stretching vibrations of Si-O-Si, deformation vibrations of O-Si-O and C-Si-O, in-plane stretching vibrations Si-O can overlaps in the 582, 814, 953 cm^{-1} range. The bands of Si-O stretching vibrations gives the reason to suggest the existence of SiO_2 network defects. At the 467 cm^{-1}, the plane stretching vibrations of Si-C observed [43].

However, the use of tetraethoxysilane as silica precursor led to the formation of surface methyl functionalized silica. This was certified by broad peak in the range 1338-1500 cm^{-1} that can be assigned to the C-H deformation vibrations of aliphatic bands [43].

2.2. The pulse chemisorption

The hydrogen pulse chemisorption data is presented in the **Table 1**.

Table 1. The data of pulse chemisorption of hydrogen

Simple	Metal dispersion, %	Metallic surface area, m^2/g metal	Concentration of active center mmol/g
5 wt. % Pd/SiO_2-C_3H_6-NH_2	5.0	21	0.017
5 wt. % Pd/SiO_2	4.3	19	0.016
5 wt. % Pd/γ-Al_2O_3	3.8	17	0.014
5 wt. % Pd/C	3.2	14	0.012

2.3. XPS of catalysts before the reaction

The surface chemical composition of silica supports determined by X-ray photoelectron spectroscopy. High resolution XPS spectra of C 1s **(Figure 3)**, N 1s **(Figure 4)**, Si 2p **(Figure 5)** are shown in appropriate figures. According to XPS data the silica contains O, C, Si elements. The synthesized amino organomodified silica contains O, C, Si and N elements.

The presence of quantities of aliphatic carbon compounds in silica is a result of inclusion aminopropyl substituent into the silica structure, incomplete hydrolysis of silane and carbon pollution. The C-N and C-Si bonds prove the inclusion of aminopropyl substituents in the silicon oxide matrix. According to the published data, the peaks at 399.5 eV and 401.6 eV in spectrum of N 1s can

Preprints (www.preprints.org) | NOT PEER-REVIEWED | Posted: 5 March 2020 doi:10.20944/preprints202003.0089.v1

Peer-reviewed version available at Catalysts 2020, 10, 375; doi:10.3390/catal10040375

attributed to C-N and N-H bonds, that correlates with the IR-spectroscopy data **(Figure 4)** [43,44].

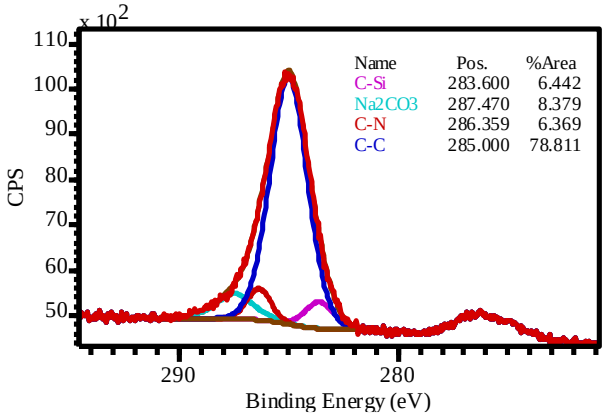

Figure 3. The high resolution XPS spectra of C 1S energy core-level of SiO_2-C_3H_6-NH_2

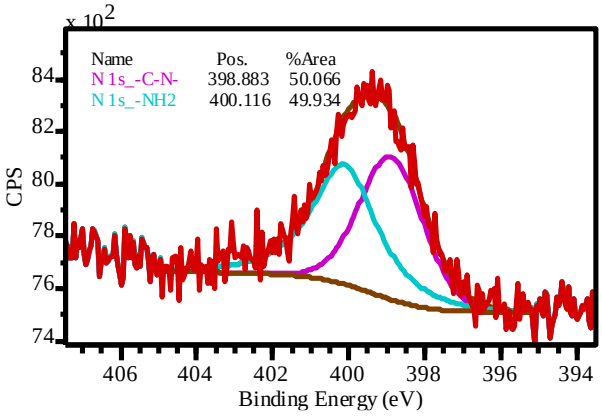

Figure 4. The high resolution XPS spectra of C 1senergy core-level of SiO_2-C_3H_6-NH_2

The bonds -C-ONa is belong to molecules of sodium carbonate **(Figure 3)** [43,44].

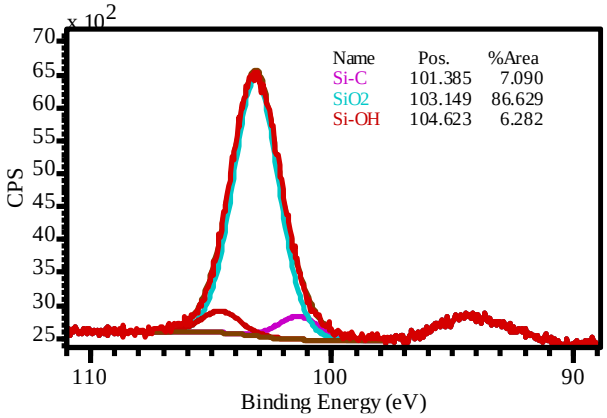

Figure 5. The high resolution XPS spectra of Si 2p energy core-level of SiO_2-C_3H_6-NH_2

The **Figure 10** shows the model decomposition of XPS high-resolution spectra of Pd 3d energy core-level of catalysts before the reaction. The atomic concentration of palladium compounds were gave in **Table 2**. The model decomposition of Pd 3d spectra for 5 wt. % Pd/γ-Al_2O_3, 5 wt. % Pd/SiO_2, 5 wt. % Pd/SiO_2-C_3H_6-NH_2 catalysts showed presence of two palladium chemical states **(Table 2, Figure 6)**. A greater number of different states of palladium were observed in the catalyst on activated carbon. In particular it was metallic palladium Pd^O, oxidized PdO on metallic Pd^O and palladium oxides PdO, PdO_2 **(Figure 6)**.

Preprints (www.preprints.org) | NOT PEER-REVIEWED | Posted: 5 March 2020 doi:10.20944/preprints202003.0089.v1

Peer-reviewed version available at Catalysts 2020, 10, 375; doi:10.3390/catal10040375

Table 2. The spectrum data of catalysts before the reaction

Catalyst	Binding energy, eV	Chemical state	at, %
5 wt. % Pd/SiO_2 [45]	334.87	Pd^0	1.47
	337.09	PdO	0.17
5 wt. % Pd/SiO_2-C_3H_6-NH_2	334.44	Pd^0	2.12
	336.59	PdO/Pd^0	0.15
5 wt. % Pd/γ-Al_2O_3 [45]	335.1	Pd^0	4.23
	337.7	PdO	0.33
5 wt. % Pd/C [45]	335.12	Pd^0	4.16
	336.20	PdO/Pd^0	1.91
	337.20	PdO	1.01
	338.48	PdO_2	0.50

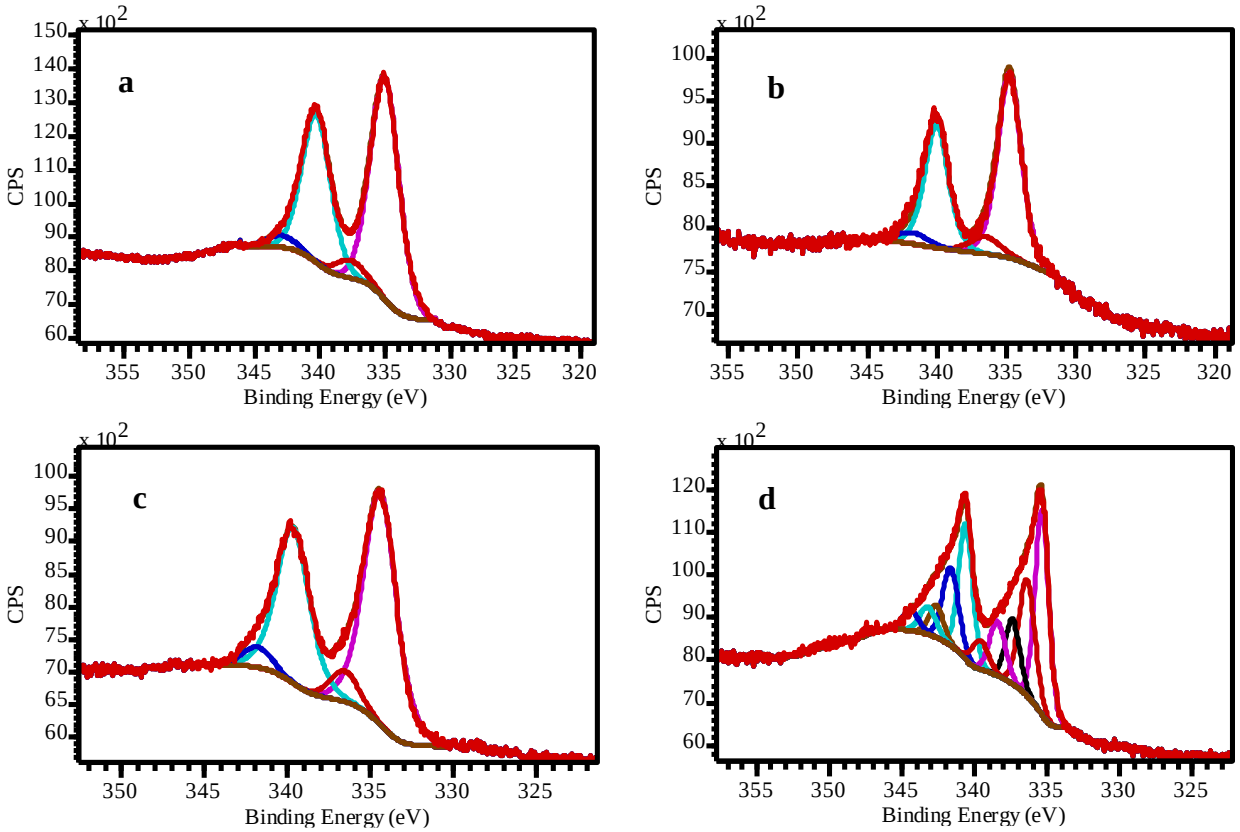

Figure 6. The model decomposition of XPS high-resolution spectra of Pd 3d energy core-level of catalysts before the reaction: a) 5 wt. % Pd/γ-Al_2O_3; b) 5 wt. % Pd/SiO_2; c) 5 wt.% Pd/SiO_2-C_3H_6-NH_2; d) 5 wt. % Pd/C;

An interesting observation was a shift of the binding energy by ~0.5 eV of palladium metal in the 5 wt. % Pd/SiO_2-C_3H_6-NH_2 catalyst. There was an assumption that this may be the result of the displacement of the electron cloud of amino groups to palladium atoms.

2.6 XPS of used catalysts

The atomic surface concentrations of palladium decrease in 5 wt. % Pd/γ-Al_2O_3, 5 wt. % Pd/SiO_2 and 5 wt. % Pd/C catalysts **(Tables 2, 3.)**. That can be attributed to metal particles diffusion into matrix of support [50]. While for amino modified sample 5 wt. % Pd/SiO_2-C_3H_6-NH_2 the change of active metal surface concentration wasn't observed. Quantity of zero valence metal in 5 wt. % Pd/SiO_2 and 5 wt. % Pd/SiO_2-C_3H_6-NH_2 samples before and after reaction did not significantly changed **(Table 3)**. The change of Pd^O surface concentrations in 5 wt. % Pd/C and Pd/γ-Al_2O_3 catalysts were the most noticeable.

Table 3. The spectrum data of catalysts after used in reaction

Catalyst	Binding energy, eV	Chemical state	At, %
5 wt. % Pd/SiO_2 [45]	335.04	Pd^0	1.04
	337.25	PdO	0.06
5 wt. % Pd/SiO_2-C_3H_6-NH_2	334.51	Pd^0	2.10
	336.50	PdO/Pd^0	0.23
5 wt. % Pd/γ-Al_2O_3 [45]	335.26	Pd^0	2.52
	337.68	PdO	0.29
5 wt. % Pd/C [45]	335.22	Pd^0	1.94
	336.12	PdO/Pd^0	2.36
	337.12	PdO	0.31
	338.00	PdO_2	1.17

In case of 5 wt. % Pd/C catalyst the quantity of PdO was decreased on 0.7 At.% and content of PdO_2 was increased on 0.7 At.% **(Tables 2, 3)**. Also, the contents of PdO and Pd^o in 5 wt. % Pd/SiO_2 and 5 wt. % Pd/γ-Al_2O_3 catalysts were decreased.

2.4. SEM

The morphology of the amino-functionalized mesoporous silica was studied by Scanning Electron Microscopy **(Figure 7)**. The synthesized silica particles have spherical shape. Average particle size diameter was found to be 1 μm before and after catalysts synthesis.

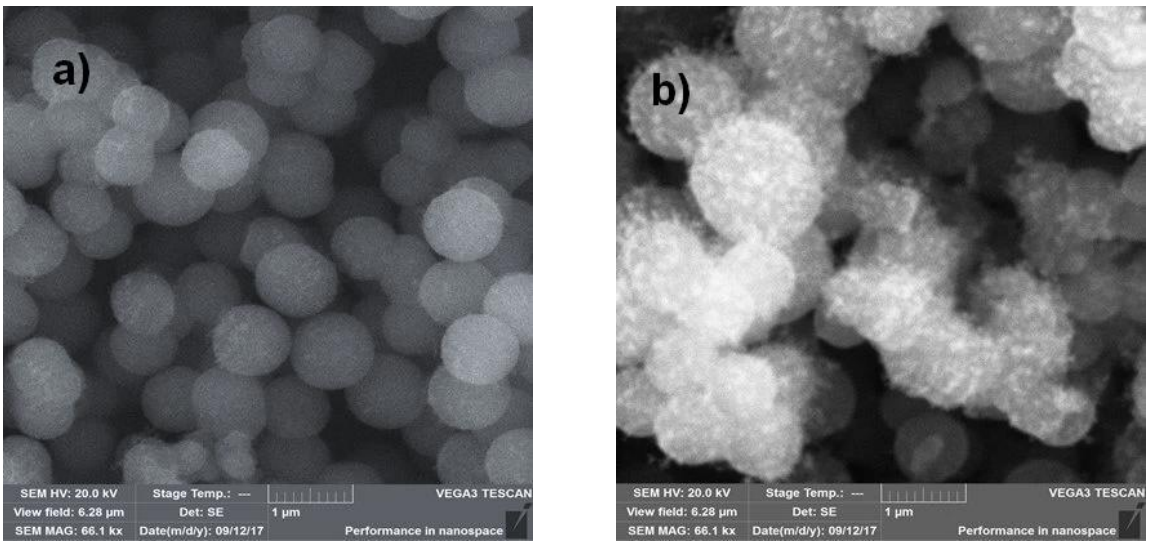

Figure 7. SEM images of a) SiO_2-C_3H_6-NH_2 and b) 5 wt. % Pd/SiO_2-C_3H_6-NH_2

2.5 TEM

The images of transmission electron microscope were obtained for reliable determination of palladium particle size **(Figure 8)**. The images show that the particles are quite different in size. The particles size in 5 wt. % Pd/SiO_2-C_3H_6-NH_2 catalyst was form 3 to 10 nm, in 5 wt. % Pd/SiO_2 catalyst was from 2 to 10 nm, in 5 wt. % Pd/γ-Al_2O_3 catalyst was form 5 to 70 nm and in 5 wt. % Pd/C catalyst was from 30 to 100 nm. In general, the data agree with the result of pulsed chemisorption. Depending on the size of the metal particles, according to both methods (microscopy and pulsed chemisorption), the catalysts can be under the following conditions: 5 wt. % Pd/γ-Al_2O_3 ≈ 5 wt. % Pd/C < 5 wt. % Pd/SiO_2 < 5 wt. % Pd/SiO_2-C_3H_6-NH_2. The TEM images with high resolution were used to analyze the atomic lattice parameters of the catalytic phase. The interplanar distance of palladium particles in 5 wt. % Pd/γ-Al_2O_3 is of the order of ~0.14 nm (220), which corresponds to the phase of metallic palladium. Other palladium particles in 5 wt. % Pd/γ-Al_2O_3 with an interplanar distance of about ~0.26 nm (111) belong to palladium oxide. The interplanar distances of ~0.14 nm (220) were observed for a catalyst of 5 wt. % Pd/SiO_2-C_3H_6-NH_2 [46-48]. The TEM data of 5 wt. % Pd/SiO_2 catalyst also show the interplanar spacings of ~0.14 nm (220) and ~0.26 nm (111) [46-48], which corresponds to the metal and oxide state of palladium. The interplanar distances of ~0.14 nm (220) and ~0.26 nm (111) were observed for a catalyst of 5 wt. % Pd/C [46-48].

Preprints (www.preprints.org) | NOT PEER-REVIEWED | Posted: 5 March 2020 doi:10.20944/preprints202003.0089.v1

Peer-reviewed version available at Catalysts 2020, 10, 375; doi:10.3390/catal10040375

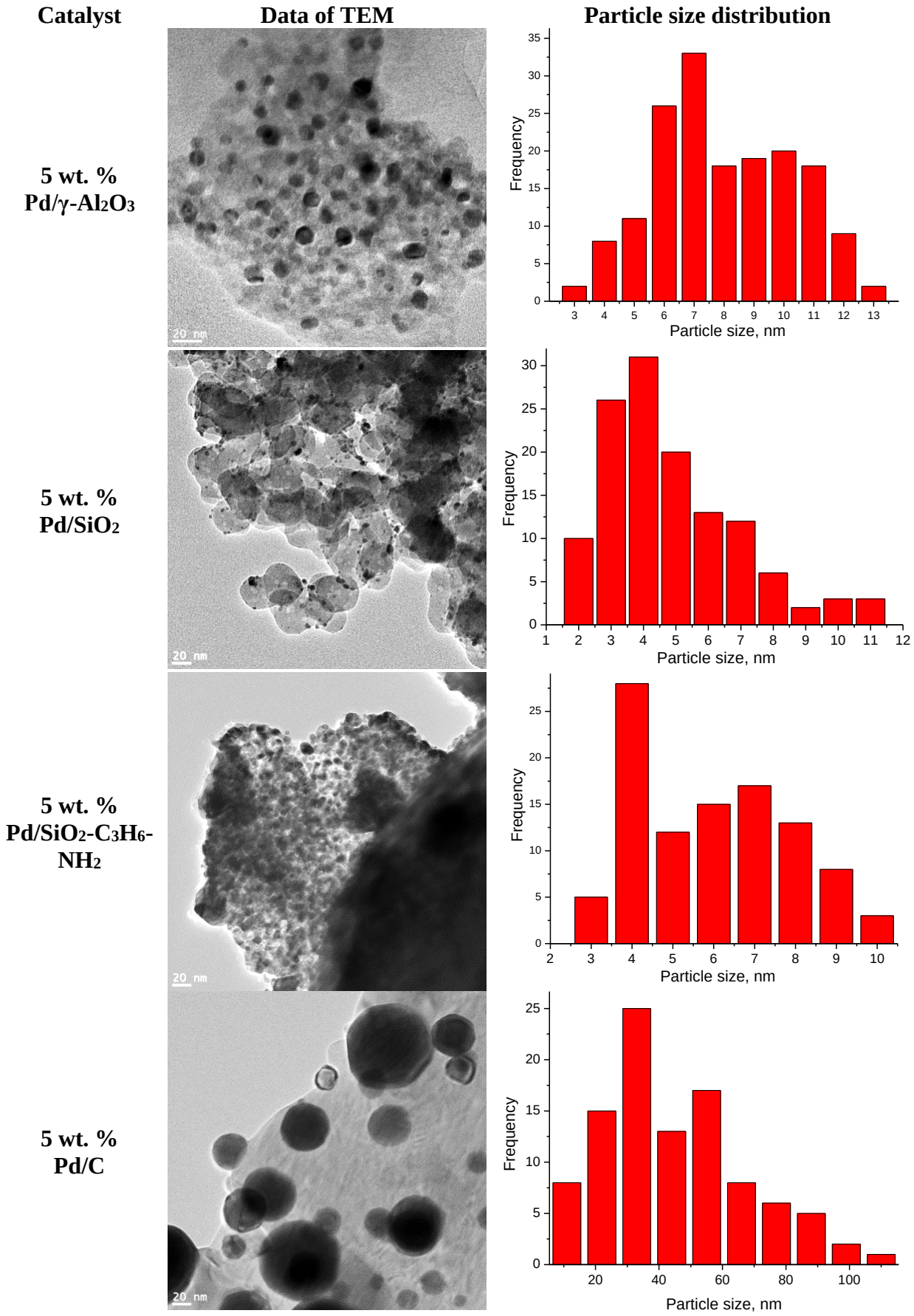

Figure 8. TEM images of catalysts and particle size distribution.

Preprints (www.preprints.org) | NOT PEER-REVIEWED | Posted: 5 March 2020 doi:10.20944/preprints202003.0089.v1

Peer-reviewed version available at Catalysts 2020, 10, 375; doi:10.3390/catal10040375

2.5. The activity of synthesized catalysts

In all cycles for all catalysts the conversion of 4-nitroaniline to 1,4-phenylenediamine was 100%. Sufficient quantity of hydrogen for completely reduce 4-nitroaniline is 3.62 mmol. Thus, according to the data of catalysts activity can arrange in the order: 5 wt. % Pd/SiO_2-C_3H_6-NH_2 (10.1 mole/sec.·10^{-5}) > Raney nickel (4.8 mole/sec.·10^{-5}) [49] > 5 wt. % Pd/C (4.4 mole/sec.·10^{-5}) ≈ 5 wt. % Pd/γ-Al_2O_3 (4.4 mole/sec.·10^{-5}) > 5 wt. % Pd/SiO_2 (0.8 mole/sec.·10^{-5}) **(Table 4)**. Comparison of the catalysts activity after catalyst recycle showed that the highest activity after five reaction cycles was observed for 5 wt. % Pd/SiO_2-C_3H_6-NH_2 **(Table 4, Figure 9)**. The catalysts stability can arrange in the following order: 5 wt. % Pd/SiO_2-C_3H_6-NH_2 > 5 wt. % Pd/SiO_2 > 5 wt. % Pd/C ≈ 5 wt. % Pd/γ-Al_2O_3.

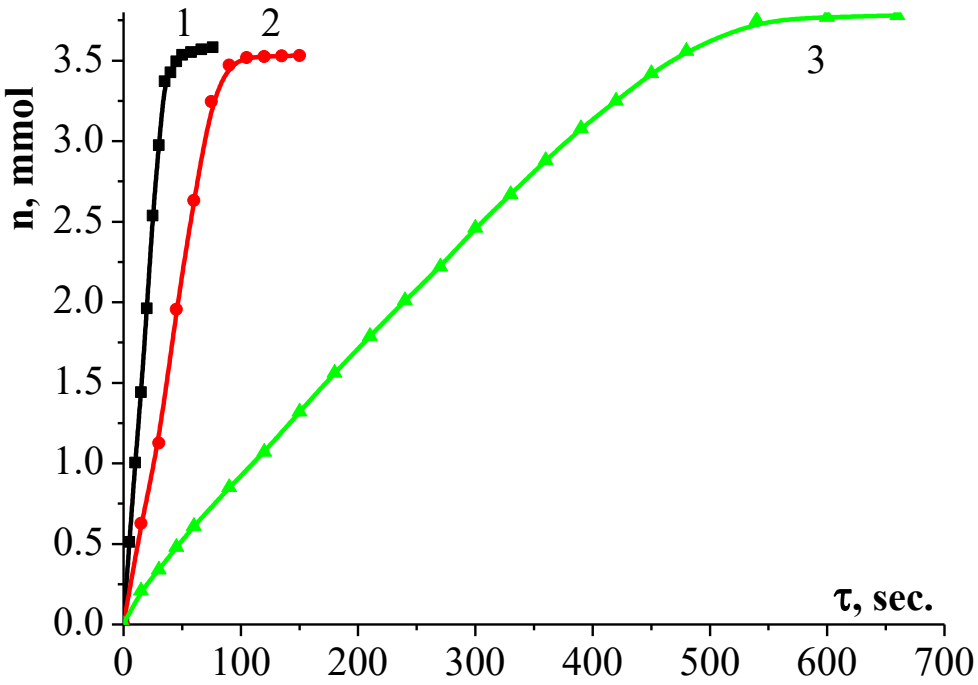

Figure 9. Kinetic curves of hydrogen uptake in the 4-nitroaniline hydrogenation in aqueous 2-propanol (0.68 mol fraction). T = 298K, $m_{(cat)}$ = 0.30 ± 0.05 g., $m_{(NA)}$ = 0.50 ± 0.05 g.

Gas chromatographic analysis made it possible to calculate the yield of 1,4-phenylenediamine in the hydrogenation reaction after each repeated addition of 4-nitroaniline **(Table 5)**. In all samples, at the end of the reaction, in each input of 4-nitroaniline traces of the starting compound were not detected, and the hydrogenation conversion of 4-nitroaniline was considered complete (100%).

Preprints (www.preprints.org) | NOT PEER-REVIEWED | Posted: 5 March 2020 doi:10.20944/preprints202003.0089.v1

Peer-reviewed version available at Catalysts 2020, 10, 375; doi:10.3390/catal10040375

Table 4. Catalytic recyclability test for successive five cycles of 4-nitroaniline hydrogenation					
Catalyst	The hydrogen consumption rate $\cdot 10^{-5}$ mole(H_2)/sec.				
	1 run	2 run	3 run	4 run	5 run
5 wt. % Pd/SiO_2-C_3H_6-NH_2	10.1	9.5	8.8	8.3	8.0
5 wt. % Pd/C [45,50]	4.5	4.1	3.9	3.5	3.2
5 wt. % Pd/SiO_2 [45,50]	0.8	0.8	0.8	0.7	0.6
5 wt. % Pd/γ-Al_2O_3 [45,50]	4.5	4.1	3.7	3.2	3.2

Analysis of the conversion rate of 4-nitroaniline and the formation of 1,4-phenylenediamine showed a similar tendency to decrease in the values of the rates, as according to the data on the consumption of hydrogen **(Table 4)**.

The second catalyst with a lower content of amino groups was obtained to confirm the effect of the amount of amino groups on the surface.

Table 5. Data of gas chromatographic analysis in hydrogenation of 4-nitroaniline to 1,4-phenylenediamine		
Catalyst	Conversion* of 4-nitroaniline	Yields* of 1,4-phenylenediamine
5 wt. % Pd/SiO_2-C_3H_6-NH_2	100	100
5 wt. % Pd/C	100	100
5 wt. % Pd/SiO_2	100	100
5 wt. % Pd/γ-Al_2O_3	100	100

*in each reaction cycle

A kinetic experiment showed that the activity of the 5 wt. % Pd/SiO_2-C_3H_6-(30 wt.%)NH_2 catalyst with an NH_2 content of 30 wt.% is two times higher than the 5 wt. % Pd/SiO_2-C_3H_6-(10 wt.%)NH_2 catalyst with a content of 10 wt.% NH_2 groups: $10.1 \cdot 10^{-5}$ mole (H_2)/sec and $5.5 \cdot 10^{-5}$ mole (H_2)/sec. Kinetic curves of hydrogen uptake of the catalytic hydrogenation of 4-nitroaniline on organically modified catalysts are shown in **Figure 10**. The higher the concentration of amino groups on the matrix surface was fixed, the more active was the palladium deposited on the silica matrix [24].

According to gas chromatography analysis the conversion of 4-nitroaniline and the yield of 1.4-phenylenediamine also amounted to 100%.

Preprints (www.preprints.org) | NOT PEER-REVIEWED | Posted: 5 March 2020 doi:10.20944/preprints202003.0089.v1

Peer-reviewed version available at Catalysts 2020, 10, 375; doi:10.3390/catal10040375

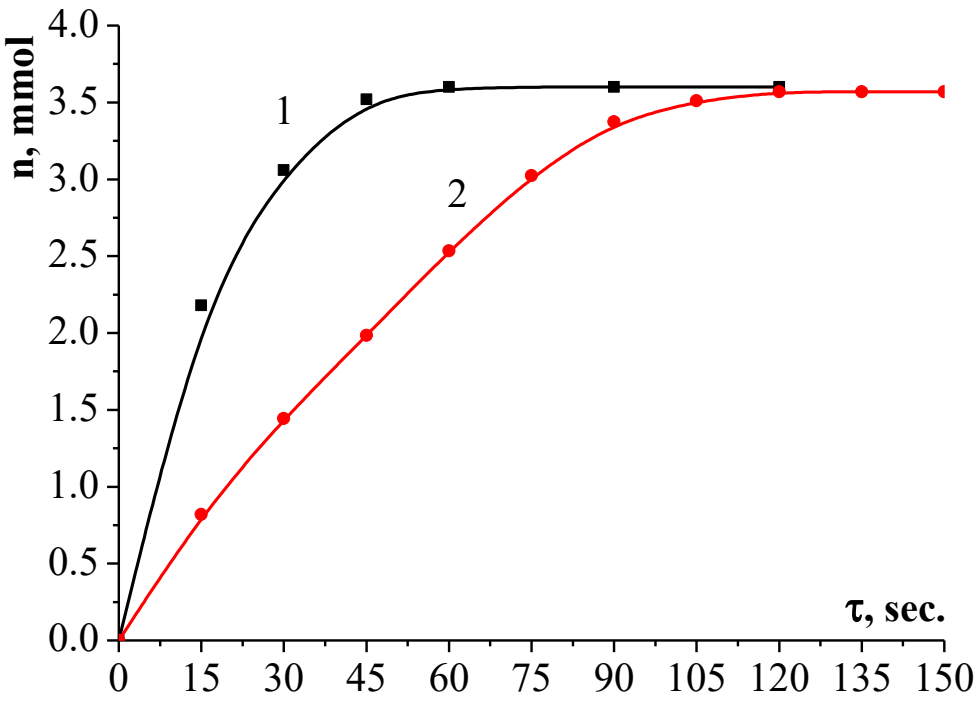

Figure 10. Kinetic curves of hydrogen uptake in the 4-nitroaniline hydrogenation in aqueous 2-propanol (0.68 mol fraction). T = 298K, $m_{(cat)}$ = 0.30 ± 0.05 g., $m_{(NA)}$ = 0.50 ± 0.05 g. 1) 5 wt. % Pd/SiO_2-C_3H_6-(30%)NH_2; 2) 5 wt. % Pd/SiO_2-C_3H_6-(10%)NH_2;

3. Materials and methods

3.1. Chemicals and materials

Tetraethoxysilane (99.9 wt.% Vecton, Russia), 2-propanol (99 wt.% Vecton, Russia) aminopropyltrimetoxysilane (97 wt.%, Sigma Aldrich, Germany), dodecyldimetylamine N-oxyde (30 wt.% solution in water, Sigma Aldrich, France), Cyclohexane (99 wt.%, ECOS-1, Russia), sodium carbonate (Vecton, Russia), hydrochloric acid (Vecton, Russia), palladium chloride ($PdCl_2 \cdot 2H_2O$, JSC "Aurat", Russia), aqueous ammonia solution (60 wt. %, Vecton, Russia) the high-purity gases (H_2 99.998%, Ar 99,99%) for the catalyst preparation were used. The γ-Al_2O_3 and activated carbon ARD-2 were purchased from Reachim Ltd. Russia and were used for catalyst synthesis as received.

3.2. Sol-gel method

3.2.1. Synthesis of silica

To synthesize spherical silica nanoparticles 700 ml of distilled water was added to 500 ml of 2-propanol in a flat-bottomed flask and solution was stirred for obtaining uniform solution. Then 200 ml of tetraethoxysilane was added to solution. The reaction mixture was kept under vigorous stirring for 30 minute with

mixing rate 1500 rpm. Subsequently, the 50 ml of aqueous ammonia solution (60 wt. %) was added dropwise to the reaction mixture during 30 min. The mixture was stirred for 2 hours with mixing rate 1000 rpm. Then, the precipitate was filtered, washed with distilled water and dried at 200 °C for 3 hours on air.

3.2.2. Synthesis of amino-functionalized silica

The first step of reaction procedure was to prepare oil/water emulsion. For this 104 ml of distillated water and 16 ml of pure ethanol were mixed at stirrer with mixing rate 1500 rpm. Then 2 ml of cyclohexane was added as co-template. After addition to of 4.8 ml of dodecyldimetylamine N-oxyde to the solution the formation of emulsion was observed. To achieve higher emulsion dispersion the mixture was treated by ultrasound for 5 minutes in ultrasonic bath 36-42 kHz, 200W. In order to homogenize the reaction mixture extra 0.2 ml of surfactant was added. Then 0.8 ml of aminopropyltrimetoxysilane was adjusted to the system for particles formation. The solution was stirred for 10 minutes at reaction temperature 60°C. Then first portion of tetraethoxysilane (1 ml) was added to the mixture and solution opalescence was immediately observed. The solution was stirred for 24 hours at room temperature. The final solution was a viscous colloid of white color, which was sufficiently stable. A vacuum filtration of solution with 0.2 micrometers membrane filter was used to separate the dispersed phase from the solution. The material was dried in vacuum oven at pressure of 0.4 bar and temperature of 100°C.

3.3 Catalyst preparation

Synthesis of Pd based catalysts was made by precipitation of palladium hydroxide due to hydrolysis reaction by addition of 3 mM H_2PdCl_6 solution in water to a 1g of support (SiO_2, γ-Al_2O_3 or activated carbon) suspended in 40 ml aqueous solution of 0.1 M Na_2CO_3 and 0.1M solution of sodium dodecyl sulfate using ultrasonic bath (Bandelin, 10P, Germany). The solution of H_2PdCl_6 was prepared in 0.2M hydrochloric acid. The suspension was mixed for 3 hours at 35°C in ultrasonic bath. The catalysts sample was filtered, thoroughly washed with distilled water and dried at 65°C under air. Prior to kinetic experiments catalysts

sample was reduced at 250°C for 60 min in the hydrogen flow in tube furnace than cooled to ambient temperature and flashed with nitrogen and immediately transferred to the catalytic reactor. Following samples were synthesized by this methodology and denoted as 5 wt. % Pd/γ-Al_2O_3, 5 wt. % Pd/SiO_2, 5 wt. % Pd/C, 5 wt. % Pd/SiO_2-C_3H_6-NH_2 with an NH_2 content of 30 wt.%.

3.4. Catalyst characterization

3.4.1. Fourier transform infrared spectroscopy (FTIR)

The diffuse reflectance IR spectroscopy was carried out using the FTIR spectrometer IRPrestige-21 (Shimadzu, Japan) equipped with a diffuse reflection attachment DRS-8000 was used for the qualitative composition of catalyst surface. The resolution of all spectra was 4 cm^{-1} and spectra were registered in the wave number range 490-4000 cm^{-1}.

3.4.2. Hydrogen pulse chemisorption

The metal dispersion and the chemically active surface area were determined due to pulse chemisorption analysis by applying a pulsed titration of the catalyst with a hydrogen. The spectra were registered on Automatic analyzer of chemosorption AutoChem HP 2950 (Micromeritics, USA).

3.4.3. XPS

X-ray photoelectron spectroscopy (XPS) data were obtained using ES-2403 spectrometer (manufacturer: Institute for Analytic Instrumentation of RAS, St. Petersburg, Russia) with anode Mg Kα (hν = 1253.6 eV), energy analyzer PHOIBOS 100-MCD5 (SPECS, Germany) and X-Ray source XR-50 (SPECS, Germany). All the data were acquired at X-ray power of 250 W. Survey spectra were recorded at an energy step of 0.5 eV with the analyzer pass energy 40 eV, and high resolution spectra were recorded at an energy step of 0.05 eV with the analyzer pass energy 7 eV. Samples were degassed within 180 min before analysis and were stable during the treatment.

3.4.4. SEM

The morphological characteristics of the amino-functionalized mesoporous silica and catalyst were examined by scanning electron microscopy (SEM,

TESCAN, Vega-LSU) equipped with X-ray microanalysis (OXFORD INCA PentaFETx3). Scanning electron microscope images were acquired at a magnification of 66.1 kX at 20 kV with SE detector.

3.4.5. TEM

The structural properties of the samples were examined using an electron microscope (JEM-2200FS, accelerating voltage 200 kV) in the transmission high-resolution electron microscopy mode (PFEM, high-resolution transmission electron microscopy - HRTEM). Model of the microscope JEOL JEM-2200FS, accelerating voltage of 200 kV. Resolution: - by points - 0.19 nm; - on the lattice - 0.1 nm; - in the mapping mode - 0.2 nm; - in the HAADF mode - 0.14 nm. For the analysis of the elemental composition, electron microscopy was used in the energy dispersive X-ray spectroscopy mode (EMF, Energy-dispersive X-ray spectroscopy - EDS).

3.4.6. Catalysts activity experiments description

The stirred reactor with the temperature-control was used to carry out of 4-nitroaniline hydrogenation to 1,4-phenylenediamine. The catalysts: 5 wt. % Pd/SiO_2-C_3H_6-NH_2, 5 wt. % Pd/SiO_2, 5 wt. % Pd/γ-Al_2O_3 and 5 wt. % Pd/C were tested in the hydrogenation of 4-nitroaniline in the environment of water solution of 2-propanol (0.68 mole fraction). Before experiments, the reactor was flushed three times with hydrogen for air removal. The reaction rates were defined by volumetric measurements of hydrogen consumption. Rates of reaction were calculated as inclination angle tangent of kinetic curves of hydrogen consumption. The test for contribution of homogeneous catalysis to the reaction rate was performed by Sheldon's filtration test methodology. After partial conversion of 4-nitroaniline, the reaction stops, the catalyst was extracted by filtration. Further the reaction was continued without catalyst, but the chemical transformation wasn't observed. Thus, the hydrogenation catalyzing only by heterogeneous catalysts.

Chromatographic analysis was performed using a gas chromatograph (Crystal, manufacturer Chromatek). The reaction rate was controlled through the 4-

nitroaniline conversion. After the process completion the catalyst was separated from the reaction mixture by centrifugation.

3.4.7. Deactivation experiments using recovered catalysts

Deactivation of catalysts was study in condition under the hydrogenation of 4-nitroaniline to 1,4-phenylenediamine in water solution of 2-propanol with repeat injecting of 4-nitroaniline at the end of reaction. The five repeated injections of 4-nitroaniline were carried out on each catalyst.

4. Conclusions

The differences in quantity of hydrogen uptake in hydrogenation on various catalysts were observed. This can relate with special interactions between hydrogen and catalysts such as adsorption, dissolvance and absorption of hydrogen. The hydrogen consumption rate for 5 wt. % Pd/SiO_2-C_3H_6-NH_2 catalyst at the same degree of conversion was in three times higher then on 5 wt. % Pd/C and 5 wt. % Pd/γ-Al_2O_3 and in six times higher than on its unmodified analogue 5 wt. % Pd/SiO_2.

The order of catalysts: 5 wt. % Pd/SiO_2-C_3H_6-NH_2 (10.1 mole/sec.·10^{-5}) > 5 wt. % Pd/C (4.4 mole/sec.·10^{-5}) ≈ 5 wt. % Pd/γ-Al_2O_3 (4.4 mole/sec.·10^{-5}) > 5 wt. % Pd/SiO_2 (0.8 mole/sec.·10^{-5}) is interconnected with XPS, Hydrogen pulse chemisorption, SEM, TEM data.

The values of metal dispersion for catalysts 5 wt. % Pd/SiO_2 and 5 wt. % Pd/γ-Al_2O_3 are very similar, thus, comparable catalytic activity could be expect. However, this is not true. The high activity of catalyst 5 wt. % Pd/γ-Al_2O_3 is associated with the crystalline structure of gamma alumina and metal particles. This is follows from the data of scanning, transmission electron microscopy.

The studying the effect of small metal particles in catalysts on differences in the values of metal dispersion, metal surface area and concentration of active centers on activity is an interesting task.

In total the concentration of active center is correlated with amount of hydrogen adsorbed under normal conditions. The only exception is 5% palladium on silica. Although a modification of the catalyst synthesis technique can correct

the result. Obviously that, the best ability of hydrogen sorption was observed in case of 5 wt. % Pd/SiO_2-C_3H_6-NH_2.

According to XPS data, the main role in catalysis belongs to metallic palladium. The greater the proportion of metallic palladium, the higher the catalytic stability of palladium. The more faulted or developed the surface structure of the carrier, the greater was the concentration of palladium on the surface and the greater activity.

In case of 5 wt. % Pd/SiO_2-C_3H_6-(30%)NH_2 and 5 wt. % Pd/SiO_2-C_3H_6-(10%)NH_2 were found the higher the concentration of amino groups on the matrix surface was fixed, the more active was the palladium deposited on the silica matrix. This confirms the hypothesis that the electron-donating properties of the amino group have a positive effect on the catalytic activity of the supported metal.

Acknowledgements

The work was funded by the Russian Science Foundation Grant No. 18-79-10157.

References

1. Gómez, J.E.; Kleij, A.W. Chapter Three - Catalytic nonreductive valorization of carbon dioxide into fine chemicals. In *Advances in Organometallic Chemistry*, Pérez, P.J., Ed. Academic Press: 2019; Vol. 71, pp. 175-226.
2. Gabriele, B. Chapter 3 - Synthesis of Heterocycles by Palladium-Catalyzed Carbonylative Reactions. In *Advances in Transition-Metal Mediated Heterocyclic Synthesis*, Solé, D., Fernández, I., Eds. Academic Press: 2018; https://doi.org/10.1016/B978-0-12-811651-7.00003-0pp. 55-127.
3. Masuda, K.; Ichitsuka, T.; Koumura, N.; Sato, K.; Kobayashi, S. Flow fine synthesis with heterogeneous catalysts. *Tetrahedron* **2018**, *74*, 1705-1730, doi:https://doi.org/10.1016/j.tet.2018.02.006.
4. Yokoi, T.; Kubota, Y.; Tatsumi, T. Amino-functionalized mesoporous silica as base catalyst and adsorbent. *Applied Catalysis A: General* **2012**, *421-422*, 14-37, doi:https://doi.org/10.1016/j.apcata.2012.02.004.
5. Hocking, M.B. 19 - PETROCHEMICALS. In *Handbook of Chemical Technology and Pollution Control*, Hocking, M.B., Ed. Academic Press: San Diego, 1998; https://doi.org/10.1016/B978-0-12-350811-9.50024-7pp. 633-664.
6. Speight, J.G. Chapter 3 - Industrial Organic Chemistry. In *Environmental Organic Chemistry for Engineers*, Speight, J.G., Ed. Butterworth-Heinemann: 2017; https://doi.org/10.1016/B978-0-12-804492-6.00003-4pp. 87-151.
7. 8 - Main industrial processes using metal oxides as catalysts or support and future trends in heterogeneous catalysis. In *Metal Oxides in Heterogeneous Catalysis*, Védrine, J.C., Ed. Elsevier: 2018; https://doi.org/10.1016/B978-0-12-811631-9.00008-9pp. 401-549.
8. Kelkar, A.A. Chapter 14 - Carbonylations and Hydroformylations for Fine Chemicals. In *Industrial Catalytic Processes for Fine and Specialty Chemicals*, Joshi, S.S., Ranade, V.V., Eds. Elsevier: Amsterdam, 2016; https://doi.org/10.1016/B978-0-12-801457-8.00014-8pp. 663-692.
9. Borah, B.J.; Mondal, M.; Bharali, P. Chapter 27 - Palladium-Based Hybrid Nanocatalysts: Application Toward Reduction Reactions. In *Noble Metal-Metal Oxide Hybrid Nanoparticles*,

Mohapatra, S., Nguyen, T.A., Nguyen-Tri, P., Eds. Woodhead Publishing: 2019; https://doi.org/10.1016/B978-0-12-814134-2.00027-9pp. 565-583.

10. Albéniz, A.C.; Casares, J.A. Chapter One - Palladium-Mediated Organofluorine Chemistry. In *Advances in Organometallic Chemistry*, Pérez, P.J., Ed. Academic Press: 2014; Vol. 62, pp. 1-110.
11. Zhang, R.; Xue, M.; Wang, B.; Ling, L. Acetylene selective hydrogenation over different size of Pd-modified Cu cluster catalysts: Effects of Pd ensemble and cluster size on the selectivity and activity. *Applied Surface Science* **2019**, *481*, 421-432, doi:https://doi.org/10.1016/j.apsusc.2019.03.006.
12. Yang, Q.; Hou, R.; Sun, K. Tuning butene selectivities by Cu modification on Pd-based catalyst for the selective hydrogenation of 1,3-butadiene. *Journal of Catalysis* **2019**, *374*, 12-23, doi:https://doi.org/10.1016/j.jcat.2019.04.018.
13. Eslava, J.L.; Gallegos-Suárez, E.; Guerrero-Ruiz, A.; Rodríguez-Ramos, I. Effect of Mo promotion on the activity and selectivity of Ru/Graphite catalysts for Fischer-Tropsch synthesis. *Catalysis Today* **2019**, https://doi.org/10.1016/j.cattod.2019.05.051, doi:https://doi.org/10.1016/j.cattod.2019.05.051.
14. He, Z.-H.; Li, N.; Wang, K.; Wang, W.-T.; Liu, Z.-T. Selective hydrogenation of quinolines over a CoCu bimetallic catalyst at low temperature. *Molecular Catalysis* **2019**, *470*, 120-126, doi:https://doi.org/10.1016/j.mcat.2019.04.005.
15. Chakoli, A.N.; Sadeghzadeh, M. Chapter 27 - Recent Trends in Biomedical and Pharmaceutical Industry Due to Engineered Nanomaterials. In *Handbook of Nanomaterials for Industrial Applications*, Mustansar Hussain, C., Ed. Elsevier: 2018; https://doi.org/10.1016/B978-0-12-813351-4.00028-6pp. 499-519.
16. Zhu, J.; Wood, J.; Deplanche, K.; Mikheenko, I.; Macaskie, L.E. Selective hydrogenation using palladium bioinorganic catalyst. *Applied Catalysis B: Environmental* **2016**, *199*, 108-122, doi:https://doi.org/10.1016/j.apcatb.2016.05.060.
17. Akti, F. The effect of potassium modification on structural properties and catalytic activity of copper and iron containing SBA-16 catalysts for selective oxidation of ethanol. *Materials Chemistry and Physics* **2019**, *227*, 21-28, doi:https://doi.org/10.1016/j.matchemphys.2019.01.054.
18. Sánchez, G.; Friggieri, J.; Keast, C.; Drewery, M.; Dlugogorski, B.Z.; Kennedy, E.; Stockenhuber, M. The effect of catalyst modification on the conversion of glycerol to allyl alcohol. *Applied Catalysis B: Environmental* **2014**, *152-153*, 117-128, doi:https://doi.org/10.1016/j.apcatb.2014.01.019.
19. Zhang, H.; Ke, D.; Cheng, L.; Feng, X.; Hou, X.; Wang, J.; Li, Y.; Han, S. CoPt-Co hybrid supported on amino modified SiO2 nanospheres as a high performance catalyst for hydrogen generation from ammonia borane. *Progress in Natural Science: Materials International* **2019**, *29*, 1-9, doi:https://doi.org/10.1016/j.pnsc.2019.01.001.
20. Fernandes, A.E.; Jonas, A.M. Design and engineering of multifunctional silica-supported cooperative catalysts. *Catalysis Today* **2018**, https://doi.org/10.1016/j.cattod.2018.11.040, doi:https://doi.org/10.1016/j.cattod.2018.11.040.
21. Feng, X.; Song, Z.; Guo, T.; Yang, R.; Liu, Y.; Chen, X.; Yang, C. Insights into the effect of surface functional groups on catalytic performance for hydrogen generation from sodium borohydride. *RSC Advances* **2016**, *6*, 113260-113266, doi:10.1039/C6RA25016E.
22. Khalili, D.; Banazadeh, A.R.; Etemadi-Davan, E. Palladium Stabilized by Amino-Vinyl Silica Functionalized Magnetic Carbon Nanotube: Application in Suzuki–Miyaura and Heck–Mizoroki Coupling Reactions. *Catalysis Letters* **2017**, *147*, 2674-2687, doi:10.1007/s10562-017-2150-1.
23. Miller, J.T.; Mojet, B.L.; Ramaker, D.E.; Koningsberger, D.C. A new model for the metal–support interaction: Evidence for a shift in the energy of the valence orbitals. *Catalysis Today* **2000**, *62*, 101-114, doi:https://doi.org/10.1016/S0920-5861(00)00412-0.
24. Jin, M.-H.; Park, J.-H.; Oh, D.; Park, J.-S.; Lee, K.-Y.; Lee, D.-W. Effect of the amine group content on catalytic activity and stability of mesoporous silica supported Pd catalysts for additive-free formic acid dehydrogenation at room temperature. *International Journal of Hydrogen Energy* **2019**, *44*, 4737-4744, doi:https://doi.org/10.1016/j.ijhydene.2018.12.208.

25. Vona, D.; Cicco, S.; Ragni, R.; Leone, G.; Lo Presti, M.; Farinola, G. Biosilica/polydopamine/silver nanoparticles composites: new hybrid multifunctional heterostructures obtained by chemical modification of Thalassiosira weissflogii silica shells. *MRS Communications* **2018**, 10.1557/mrc.2018.103, 1-7, doi:10.1557/mrc.2018.103.
26. Gupta, R.K.; Kusuma, D.Y.; Lee, P.S.; Srinivasan, M.P. Covalent Assembly of Gold Nanoparticles for Nonvolatile Memory Applications. *ACS Applied Materials & Interfaces* **2011**, *3*, 4619-4625, doi:10.1021/am201022v.
27. Alvarez-Toral, A.; Fernández, B.; Malherbe, J.; Claverie, F.; Pecheyran, C.; Pereiro, R. Synthesis of amino-functionalized silica nanoparticles for preparation of new laboratory standards. *Spectrochimica Acta Part B: Atomic Spectroscopy* **2017**, *138*, 1-7, doi:https://doi.org/10.1016/j.sab.2017.10.002.
28. Sugimura, H.; Hanji, T.; Takai, O.; Masuda, T.; Misawa, H. Photolithography based on organosilane self-assembled monolayer resist. *Electrochimica Acta* **2001**, *47*, 103-107, doi:https://doi.org/10.1016/S0013-4686(01)00554-0.
29. Pasquardini, L.; Lunelli, L.; Potrich, C.; Marocchi, L.; Fiorilli, S.; Vozzi, D.; Vanzetti, L.; Gasparini, P.; Anderle, M.; Pederzolli, C. Organo-silane coated substrates for DNA purification. *Applied Surface Science* **2011**, *257*, 10821-10827, doi:https://doi.org/10.1016/j.apsusc.2011.07.112.
30. Oliveira, R.L.; He, W.; Klein Gebbink, R.J.M.; de Jong, K.P. Palladium nanoparticles confined in thiol-functionalized ordered mesoporous silica for more stable Heck and Suzuki catalysts. *Catalysis Science & Technology* **2015**, *5*, 1919-1928, doi:10.1039/C4CY01517G.
31. Hajipour, A.R.; Mohammadsaleh, F. Triazole-Functionalized Silica Supported Palladium(II) Complex: A Novel and Highly Active Heterogeneous Nano-catalyst for C–C Coupling Reactions in Aqueous Media. *Catalysis Letters* **2018**, *148*, 1035-1046, doi:10.1007/s10562-018-2316-5.
32. Yuan, M.; Yang, R.; Wei, S.; Hu, X.; Xu, D.; Yang, J.; Dong, Z. Ultra-fine Pd nanoparticles confined in a porous organic polymer: A leaching-and-aggregation-resistant catalyst for the efficient reduction of nitroarenes by NaBH4. *Journal of Colloid and Interface Science* **2019**, *538*, 720-730, doi:https://doi.org/10.1016/j.jcis.2018.11.065.
33. Bourane, A.; Elanany, M.; Pham, T.V.; Katikaneni, S.P. An overview of organic liquid phase hydrogen carriers. *International Journal of Hydrogen Energy* **2016**, *41*, 23075-23091, doi:https://doi.org/10.1016/j.ijhydene.2016.07.167.
34. Schrimpf, M.; Esteban, J.; Rösler, T.; Vorholt, A.J.; Leitner, W. Intensified reactors for gas-liquid-liquid multiphase catalysis: From chemistry to engineering. *Chemical Engineering Journal* **2019**, *372*, 917-939, doi:https://doi.org/10.1016/j.cej.2019.03.133.
35. Song, J.; Huang, Z.-F.; Pan, L.; Li, K.; Zhang, X.; Wang, L.; Zou, J.-J. Review on selective hydrogenation of nitroarene by catalytic, photocatalytic and electrocatalytic reactions. *Applied Catalysis B: Environmental* **2018**, *227*, 386-408, doi:https://doi.org/10.1016/j.apcatb.2018.01.052.
36. Huang, T.; Fu, Y.; Peng, Q.; Yu, C.; Zhu, J.; Yu, A.; Wang, X. Catalytic hydrogenation of p-nitrophenol using a metal-free catalyst of porous crimped graphitic carbon nitride. *Applied Surface Science* **2019**, *480*, 888-895, doi:https://doi.org/10.1016/j.apsusc.2019.03.035.
37. Sharma, S. Metal dependent catalytic hydrogenation of nitroarenes over water-soluble glutathione capped metal nanoparticles. *Journal of Colloid and Interface Science* **2015**, *441*, 25-29, doi:https://doi.org/10.1016/j.jcis.2014.11.030.
38. Fu, Y.; Qin, L.; Huang, D.; Zeng, G.; Lai, C.; Li, B.; He, J.; Yi, H.; Zhang, M.; Cheng, M., et al. Chitosan functionalized activated coke for Au nanoparticles anchoring: green synthesis and catalytic activities in hydrogenation of nitrophenols and azo dyes. *Applied Catalysis B: Environmental* **2019**, https://doi.org/10.1016/j.apcatb.2019.05.042, doi:https://doi.org/10.1016/j.apcatb.2019.05.042.
39. Zarrintaj, P.; Bakhshandeh, B.; Saeb, M.R.; Sefat, F.; Rezaeian, I.; Ganjali, M.R.; Ramakrishna, S.; Mozafari, M. Oligoaniline-based conductive biomaterials for tissue engineering. *Acta Biomaterialia* **2018**, *72*, 16-34, doi:https://doi.org/10.1016/j.actbio.2018.03.042.
40. Amer, I.; Mokrani, T.; Jewell, L.; Young, D.A.; Vosloo, H.C.M. Oxidative copolymerization of p-phenylenediamine and 3-aminobenzenesulfonic acid. *Tetrahedron Letters* **2016**, *57*, 426-430, doi:https://doi.org/10.1016/j.tetlet.2015.12.056.

41. Jin, J.-s.; Ning, Y.-y.; Hu, K.; Wu, H.; Zhang, Z.-t. Solubility of p-Nitroaniline in Supercritical Carbon Dioxide with and without Mixed Cosolvents. *Journal of Chemical & Engineering Data* **2013**, *58*, 1464-1469, doi:10.1021/je300987d.
42. Nishioka, R.; Hiasa, T.; Kimura, K.; Onishi, H. Specific Hydration on p-Nitroaniline Crystal Studied by Atomic Force Microscopy. *The Journal of Physical Chemistry C* **2013**, *117*, 2939-2943, doi:10.1021/jp3117424.
43. Scaffaro, R.; Botta, L.; Lo Re, G.; Bertani, R.; Milani, R.; Sassi, A. Surface modification of poly(ethylene-co-acrylic acid) with amino-functionalized silica nanoparticles. *Journal of Materials Chemistry* **2011**, *21*, 3849-3857, doi:10.1039/C0JM03310C.
44. Jakša, G.; Štefane, B.; Kovač, J. XPS and AFM characterization of aminosilanes with different numbers of bonding sites on a silicon wafer. *Surface and Interface Analysis* **2013**, *45*, 1709-1713, doi:10.1002/sia.5311.
45. Latypova, A.; Tarasyuk, I.; Filippov, D.; Lefedova, O.; Bykov, A.; Sidorov, A.; Doluda, V.; Sulman, E. Synthesis, stability and activity of palladium supported over various inorganic matrices in the selective hydrogenation of nitroaniline. *Reaction Kinetics, Mechanisms and Catalysis* **2019**, 10.1007/s11144-019-01590-0, doi:10.1007/s11144-019-01590-0.
46. Zhang, D.; Jin, C.; Tian, H.; Xiong, Y.; Zhang, H.; Qiao, P.; Fan, J.; Zhang, Z.; Li, Z.Y.; Li, J. An In situ TEM study of the surface oxidation of palladium nanocrystals assisted by electron irradiation. *Nanoscale* **2017**, *9*, 6327-6333, doi:10.1039/C6NR08763A.
47. Chen, A.; Ostrom, C. Palladium-Based Nanomaterials: Synthesis and Electrochemical Applications. *Chemical Reviews* **2015**, *115*, 11999-12044, doi:10.1021/acs.chemrev.5b00324.
48. Blosi, M.; Ortelli, S.; Costa, A.L.; Dondi, M.; Lolli, A.; Andreoli, S.; Benito, P.; Albonetti, S. Bimetallic Nanoparticles as Efficient Catalysts: Facile and Green Microwave Synthesis. *Materials (Basel)* **2016**, *9*, 550, doi:10.3390/ma9070550.
49. Kha, N.T.T.; Merkin, A.A.; Komarov, A.A.; Korpatenkov, D.O.; Lefedova, O.V. Kinetics of catalytic hydrogenation of 4-nitroaniline in aqueous solutions of propan-2-ol with acid or base additives. *Russian Journal of Physical Chemistry A* **2014**, *88*, 588-590, doi:10.1134/S0036024414040189.
50. Latypova, A.R.; Tarasyuk, I.A.; Filippov, D.V.; Lefedova, O.V.; Bykov, A.V.; Sidorov, A.I.; Doluda, V.Y.; Sulman, E.M. Synthesis, stability and activity of palladium supported over various inorganic matrices in the selective hydrogenation of nitroaniline. *Reaction Kinetics, Mechanisms and Catalysis* **2019**, *127*, 741-755, doi:10.1007/s11144-019-01590-0.